



# Phosphate removal from aqueous solutions using polyaniline/ $\text{Ni}_{0.5}\text{Zn}_{0.5}\text{Fe}_2\text{O}_4$ magnetic nanocomposite

Mohammad Hossein Tarmahi<sup>1</sup>, Farid Moeinpour<sup>2\*</sup>

<sup>1</sup>MSc in Water and Wastewater Engineering, Department of Chemistry, College of Science, Bandar Abbas Branch, Islamic Azad University, Bandar Abbas, Iran

<sup>2</sup>Assistant Professor of Chemistry, Department of Chemistry, College of Science, Bandar Abbas Branch, Islamic Azad University, Bandar Abbas, Iran

## Abstract

**Background:** Phosphorus is an indispensable element for the growth of animals and plants. There are several environmental problems related to phosphate; therefore, the technical and economic methods of removing phosphate are of great importance. This study evaluated the efficiency of polyaniline/ $\text{Ni}_{0.5}\text{Zn}_{0.5}\text{Fe}_2\text{O}_4$  magnetic nanocomposite in removing phosphate from aqueous environments.

**Methods:** The adsorbent was characterized by several methods, including X-ray diffraction (XRD), scanning electron microscopy (SEM), vibrating sample magnetometer (VSM), and Fourier transform infrared (FT-IR) spectroscopy. Then, the potential of the adsorbent to adsorb phosphate was investigated. The effects of the parameters of contact time (5-60 minutes), pH (3-9), adsorbent dosage (0.05-0.6 g), and initial phosphate concentration (2-100 mg/L) on the phosphate removal yield were studied. All phosphate ion concentrations were measured using the ammonium molybdate spectrophotometric method.

**Results:** The results showed that a time of 30 minutes, pH of 5, and adsorbent dose of 0.4 g were the optimum conditions for phosphate removal through adsorption. Increasing the initial concentration of phosphate from 2 to 100 mg/L decreased the removal efficiency from 90.3% to 32%. The experimental data was fitted well with the Freundlich isotherm model ( $R^2 = 0.997$ ).

**Conclusion:** Polyaniline/ $\text{Ni}_{0.5}\text{Zn}_{0.5}\text{Fe}_2\text{O}_4$  magnetic nanocomposite removes phosphate from aqueous solutions with a simple and environmentally benign procedure. The maximum adsorption capacity based on Langmuir isotherm ( $R^2 = 0.931$ ) is 85.4 mg/g. This magnetic nanocomposite is applicable in managing water resource pollution caused by phosphate ions.

**Keywords:** Adsorption, Phosphates, Nanocomposites, Polyaniline

**Citation:** Tarmahi MH, Moeinpour F. Phosphate removal from aqueous solutions using polyaniline/ $\text{Ni}_{0.5}\text{Zn}_{0.5}\text{Fe}_2\text{O}_4$  magnetic nanocomposite. Environmental Health Engineering and Management Journal 2017; 4(2): 65–71. doi: 10.15171/EHEM.2017.10.

## Article History:

Received: 5 October 2016

Accepted: 8 January 2017

ePublished: 30 January 2017

## \*Correspondence to:

Farid Moeinpour

Email: fmoeinpour52@iauba.ac.ir

## Introduction

Adsorption has been established as an important and economically practical treatment technology for removing phosphate ions from water and wastewater. Activated carbon is the most common adsorbent used for this purpose. Despite the abundance of applications for activated carbon, its uses are sometimes limited by its high cost and loss during reformation (1-4). Therefore, researchers are seeking new low-cost substitute adsorbents for water pollution control, especially where cost plays an important role. Many efforts have been made to develop other adsorbents that are effective and inexpensive. They can be produced from a wide variety of raw materials which are abundant and have high carbon and low inorganic content. Because of the low cost and high accessibility of these materials it is not essential to have complex regeneration processes; inexpensive adsorption methods

have attracted the attention of many researchers. Often, the adsorption capabilities of such adsorbents are not great; therefore, studies of more and more new adsorbents are still being developed. Some inexpensive adsorbents used to remove phosphate ions have been studied, such as fly ash (5), red mud (6), aluminum hydroxide (7), iron oxide (8), zirconium oxide (9), manganese dioxide (10), modified clinoptilolite (11) and horizontal roughing filters (12).

In recent years, economic problems have encouraged the creation of inexpensive, efficient alternative methods of wastewater treatment. Use of magnetic adsorbents is one of the most efficient, technical, and economic methods of treating wastewater. These adsorbents have magnetic properties and, by using an external magnetic field, can be easily separated from solutions. In magnetic separation, the usual high costs of separation, e.g., centrifugation



and filtration, are not incurred (13). Extensive research has been done into the magnetization of materials such as chitosan (14), silica (15), polymer (16), and activated carbon (17) for water contaminant removal. The use of this property in nanoparticles is remarkable because of their high specific surface area and adsorption capacities (18). Nickel-zinc ferrites have drawn noticeable consideration from researchers because of their remarkable magnetic properties, large permeability, and very high electrical resistivity (19). They have an extensive list of potential applications in such areas as high-density information storage devices, microwave devices, transformer cores, magnetic fluids (20), etc. This study investigated the capability of  $\text{Ni}_{0.5}\text{Zn}_{0.5}\text{Fe}_2\text{O}_4$  magnetic nanoparticles that were surface-modified with polyaniline (PANI) and used a polyaromatic amine as an effective adsorbent for removing phosphate from aqueous solutions (Figure 1). PANI, a familiar conducting polymer, is one of the most conceivably useful conducting polymers. It has received significant consideration by many researchers (21-23). PANI may be readily synthesized chemically or electrochemically from acidic aqueous solutions (24,25). The chemical structure of PANI is shown in Figure 2.

## Methods

### Materials

Anhydrous potassium dihydrogen orthophosphate ( $\text{KH}_2\text{PO}_4$ ) was purchased from Merck. A 1000 ppm stock solution of the  $\text{KH}_2\text{PO}_4$  was provided in deionized water. All solutions used in this study were made by consecutive diluting with double distilled water. All chemicals [ $\text{Fe}(\text{NO}_3)_3 \cdot 9\text{H}_2\text{O}$ ,  $\text{Zn}(\text{NO}_3)_2 \cdot 6\text{H}_2\text{O}$  and  $\text{Ni}(\text{NO}_3)_2 \cdot 6\text{H}_2\text{O}$ ,  $\text{NaOH}$  and  $\text{HNO}_3$ ] were of analytical grade and obtained from Sigma-Aldrich. X-ray diffraction analysis (XRD) was carried out using a PAN analytical X'Pert Pro X-ray diffractometer. Surface morphology and particle size were investigated with a Hitachi S-4800 scanning electron microscopy (SEM) instrument. Infrared (IR) spectra of the samples were obtained with a Bruker model 470 Fourier transform infrared (FT-IR) spectrometer. Concentrations of phosphate ion solutions were analyzed using the ammonium molybdate spectrophotometric method.

### Synthesis of $\text{Ni}_{0.5}\text{Zn}_{0.5}\text{Fe}_2\text{O}_4/\text{PANI}$

$\text{Ni}_{0.5}\text{Zn}_{0.5}\text{Fe}_2\text{O}_4$  nanoparticles were initially prepared using stoichiometric ratios of metal nitrates and freshly extracted

egg-white (26). The metal nitrates [ $\text{Fe}(\text{NO}_3)_3 \cdot 9\text{H}_2\text{O}$ ,  $\text{Zn}(\text{NO}_3)_2 \cdot 6\text{H}_2\text{O}$  and  $\text{Ni}(\text{NO}_3)_2 \cdot 6\text{H}_2\text{O}$ ] were dissolved together in a minimum amount of double-distilled water to obtain a clear solution. Sixty milliliters of extracted egg-white was dissolved in 40 mL of double-distilled water by vigorous stirring and was added to the nitrate mixture at ambient temperature. After constant stirring for 30 minutes, the resultant sol-gel was evaporated at 353 K until dry precursor was obtained. The dried precursors were ground and calcined in a muffle furnace at 823 K for 2 hours. The  $\text{PANI-Ni}_{0.5}\text{Zn}_{0.5}\text{Fe}_2\text{O}_4$  composite was prepared by precipitating PANI on the surface of pre-synthesized  $\text{Ni}_{0.5}\text{Zn}_{0.5}\text{Fe}_2\text{O}_4$  nanoparticles. In this method, 50 mL of freshly prepared reaction mixture (0.1 M aniline, 0.125 M ammonium peroxydisulfate in 0.5 M nitric acid) was added to 1.6 g of  $\text{Ni}_{0.5}\text{Zn}_{0.5}\text{Fe}_2\text{O}_4$  at room temperature (27). The mixture was stirred during the polymerization of aniline, which was completed within 1 hour. Next, the  $\text{Ni}_{0.5}\text{Zn}_{0.5}\text{Fe}_2\text{O}_4/\text{PANI}$  nanocomposite was magnetically separated, washed with 0.5 M nitric acid and with acetone, and finally dried at 333 K in a vacuum oven for 6 hours.

### Batch adsorption experiments

Phosphate adsorption ions onto  $\text{Ni}_{0.5}\text{Zn}_{0.5}\text{Fe}_2\text{O}_4/\text{PANI}$  was studied in aqueous phosphate solutions under diverse practical conditions (pHs = 3–9) at 298 K and 5 mg/L phosphate ion solution. 0.10 g  $\text{Ni}_{0.5}\text{Zn}_{0.5}\text{Fe}_2\text{O}_4/\text{PANI}$  was added to 50 mL of phosphate solution. After that, the resultant mixture was shaken in a shaker at 1000 rpm. The initial pHs of the phosphate solutions were balanced in the range of 3 to 9 with 0.1 mol/L  $\text{HNO}_3$  or 0.1 mol/L  $\text{NaOH}$  solutions by a pH meter. When equilibrium was reached, the solutions were centrifuged and the  $\text{Ni}_{0.5}\text{Zn}_{0.5}\text{Fe}_2\text{O}_4/\text{PANI}$  was magnetically removed. The concentration of phosphate ions in the supernatant was measured spectrophotometrically using the ammonium molybdate method. The effects of various parameters (contact time, initial phosphate concentration, pH,  $\text{Ni}_{0.5}\text{Zn}_{0.5}\text{Fe}_2\text{O}_4/$

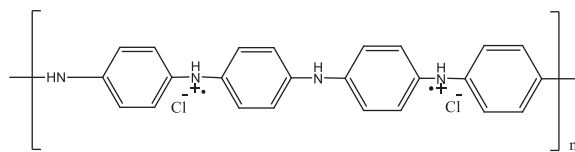


Figure 2. Chemical structure of acid doped synthesized PANI.

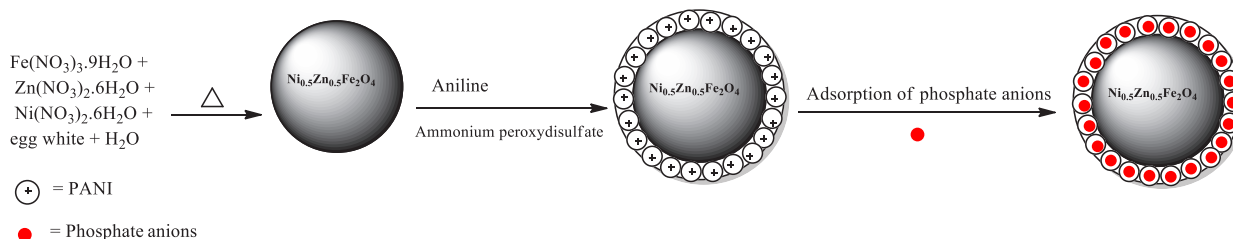


Figure 1. Formation process of  $\text{Ni}_{0.5}\text{Zn}_{0.5}\text{Fe}_2\text{O}_4/\text{PANI}$  and its application as a phosphate adsorbent.

PANI dose, and temperature) on phosphate removal were studied.

Phosphate removal (%R) was computed using Eq. (1):

$$\%R = \frac{C_0 - C_t}{C_0} \times 100 \quad (1)$$

where  $C_0$  and  $C_t$  (mg/L) are initial phosphate concentration and time  $t$ , respectively.

The adsorption capacity of the adsorbent ( $Q_e$ ) was computed by Eq. (2):

$$Q_e = \frac{(C_0 - C_e)V}{m} \quad (2)$$

where  $C_0$  and  $C_e$  are the initial and equilibrium concentrations of the phosphate (mg/L), respectively,  $m$  is the mass of the adsorbent (g), and  $V$  is the volume of phosphate solution (L).

### Adsorption Isotherms

For adsorption equilibrium studies, 0.40 g of  $\text{Ni}_{0.5}\text{Zn}_{0.5}\text{Fe}_2\text{O}_4/\text{PANI}$  was added to 50 mL of different concentrations of phosphate solutions (2-100 mg/L and pH = 5) at 298 K. These solutions were shaken at 1000 rpm for 30 minutes. After adsorption, the concentrations of the phosphate solutions were analyzed on a UV-Vis spectrophotometer using the ammonium molybdate method.

### Results

In this section, the results of this study are presented in the form of diagrams and tables.  $\text{Ni}_{0.5}\text{Zn}_{0.5}\text{Fe}_2\text{O}_4/\text{PANI}$  nanocrystallites were specified by FT-IR spectroscopy (Figure 3), XRD (Figure 4), SEM (Figure 5), and VSM (Figure 6). Figure 7 shows the different contact times, removal efficiency of the remaining phosphate, and the adsorption equilibrium time. As shown in Figure 7, removal efficiency increased in the time range of 0 to 30 minutes, became fixed at 30 minutes and partly increased at 60 minutes. Thus, the adsorption equilibrium time was determined to be 30 minutes in this test.

The effect of solution pH (from 3 to 9) on phosphate removal was studied at 298 K. Figure 8 shows the removal efficiency of phosphate at the equilibrium time and at 4

different pHs (3, 5, 7, and 9), equaling, respectively, 78%, 82%, 77.5%, and 56%. Maximum adsorption occurred at around pH 5.0, and this value was therefore selected for all adsorption experiments in this study.

The effect of  $\text{Ni}_{0.5}\text{Zn}_{0.5}\text{Fe}_2\text{O}_4/\text{PANI}$  dosage on phosphate adsorption was investigated with various adsorbent doses (from 0.05 to 0.60 g). The results are exhibited in Figure 8. The greatest adsorption of phosphate was about 89.0%, achieved when applying a  $\text{Ni}_{0.5}\text{Zn}_{0.5}\text{Fe}_2\text{O}_4/\text{PANI}$  dosage of 0.40 g in 50 mL of 5 mg/L phosphate solution.

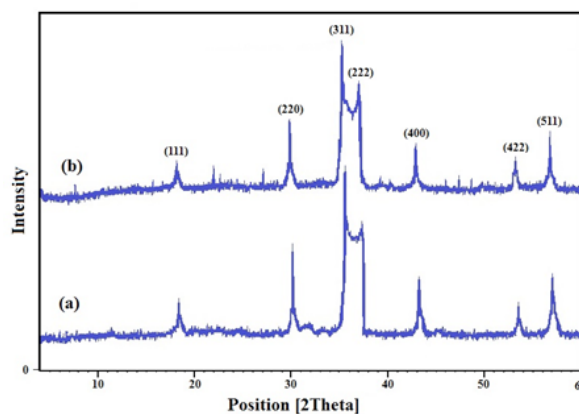


**Figure 4.** XRD patterns of  $\text{Ni}_{0.5}\text{Zn}_{0.5}\text{Fe}_2\text{O}_4$ . (a) Synthesized  $\text{Ni}_{0.5}\text{Zn}_{0.5}\text{Fe}_2\text{O}_4$ ; (b) Standard  $\text{Ni}_{0.5}\text{Zn}_{0.5}\text{Fe}_2\text{O}_4$  (JCPDS 08-0234).

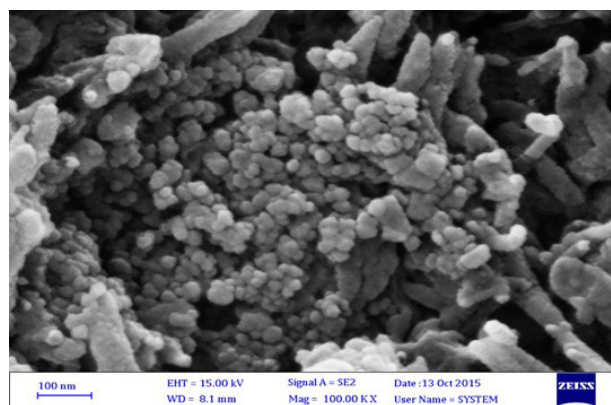


**Figure 5.** SEM image of  $\text{Ni}_{0.5}\text{Zn}_{0.5}\text{Fe}_2\text{O}_4/\text{PANI}$  nanocomposite.

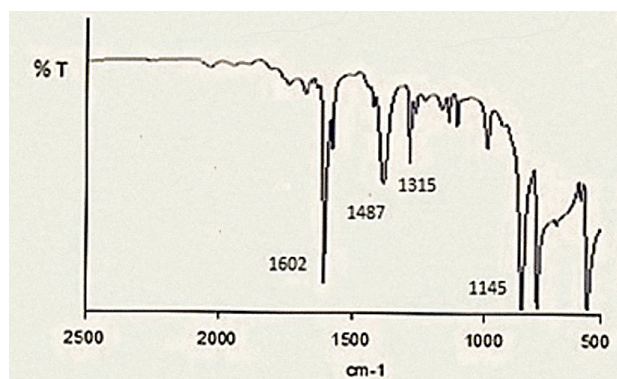


**Figure 3.** FT-IR spectrum of  $\text{Ni}_{0.5}\text{Zn}_{0.5}\text{Fe}_2\text{O}_4/\text{PANI}$ .

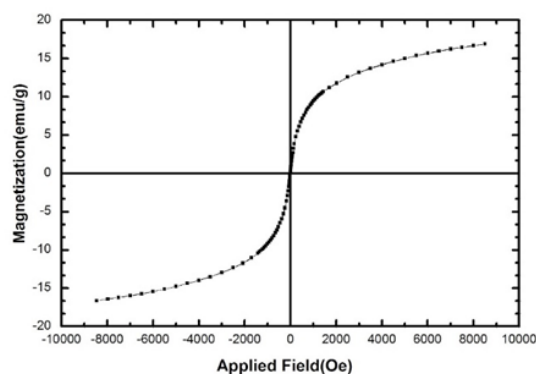


**Figure 6.** VSM curve of  $\text{Ni}_{0.5}\text{Zn}_{0.5}\text{Fe}_2\text{O}_4/\text{PANI}$  at room temperature.

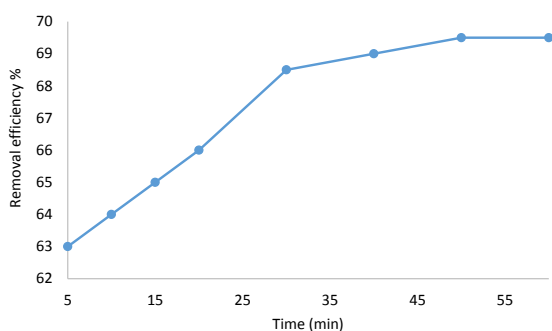


Figure 7. Effect of contact time.

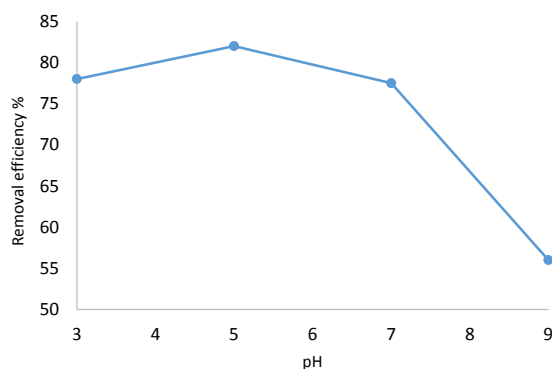


Figure 8. Effect of pH on phosphate removal.

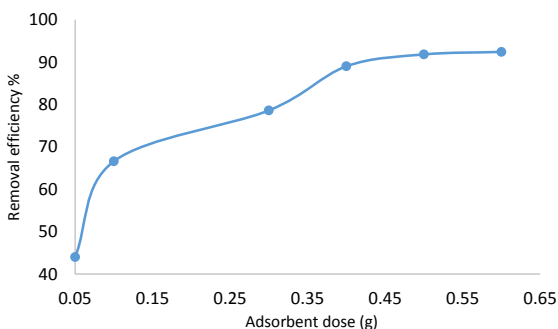


Figure 9. Effect of adsorbent dosage on phosphate removal.

Batch adsorption experiments were performed at different initial phosphate concentrations (2, 5, 10, 30, 50, and 100 mg/L) while other experimental parameters were kept constant. Figure 9 shows that the percentage of phosphate removal (%R) decreased when the initial concentration was increased, indicating that the adsorption of phosphate onto  $\text{Ni}_{0.5}\text{Zn}_{0.5}\text{Fe}_2\text{O}_4/\text{PANI}$  is highly related to initial phosphate concentration.

The adsorption isotherms of phosphate by the adsorbent are shown in Table 1. As can be seen,  $R^2 = 0.931$  in the Langmuir model,  $R^2 = 0.997$  in the Freundlich model, and  $R^2 = 0.687$  in the Dubinin–Radushkevich model.

## Discussion

In this study, the SEM technique was used to perform morphological analyses and characterize the size and shape

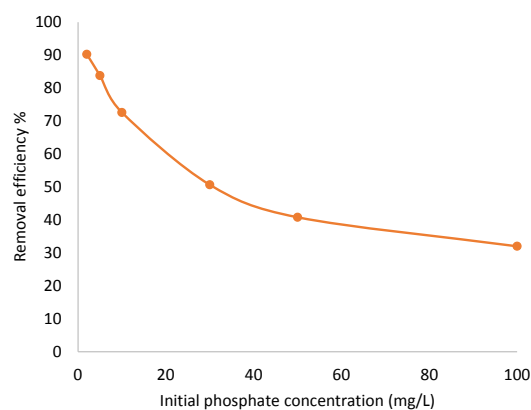


Figure 10. Effect of initial phosphate concentration on removal efficiency of phosphate.

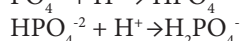
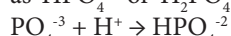
of the resultant  $\text{Ni}_{0.5}\text{Zn}_{0.5}\text{Fe}_2\text{O}_4/\text{PANI}$  nanocomposites. XRD was used to estimate the morphologic type of  $\text{Ni}_{0.5}\text{Zn}_{0.5}\text{Fe}_2\text{O}_4/\text{PANI}$ . Functional group analyses of  $\text{Ni}_{0.5}\text{Zn}_{0.5}\text{Fe}_2\text{O}_4/\text{PANI}$  were performed using the FT-IR technique. The magnetic properties of the  $\text{Ni}_{0.5}\text{Zn}_{0.5}\text{Fe}_2\text{O}_4/\text{PANI}$  were evaluated with a VSM.

$\text{Ni}_{0.5}\text{Zn}_{0.5}\text{Fe}_2\text{O}_4$  nanocrystallites were prepared according to the procedure reported by Gabal et al (26). Nano  $\text{Ni}_{0.5}\text{Zn}_{0.5}\text{Fe}_2\text{O}_4/\text{PANI}$  were characterized by FT-IR (Figure 3). In the FT-IR spectrum of  $\text{Ni}_{0.5}\text{Zn}_{0.5}\text{Fe}_2\text{O}_4/\text{PANI}$ , many of the  $\text{Ni}_{0.5}\text{Zn}_{0.5}\text{Fe}_2\text{O}_4$  and PANI bands, with some having a slight shift, are distinct, which shows that PANI well coated the  $\text{Ni}_{0.5}\text{Zn}_{0.5}\text{Fe}_2\text{O}_4$ . The peaks in the range of 500–1000  $\text{cm}^{-1}$  were caused by the  $\text{Fe}_3\text{O}_4$  framework, which is in accordance with the iron oxide spectrum (28). The peaks at 1602 and 1487  $\text{cm}^{-1}$  were attributed to the characteristic C = C stretching of the quinoid and benzenoid rings; the peaks at 1315  $\text{cm}^{-1}$  were assigned to the C – N stretching of the benzenoid ring; and the broad peak at 1145  $\text{cm}^{-1}$  were related to the vibration mode of N=Q=N (Q refers to the quinonic-type rings) (29,30). This apparently shows that the  $\text{Ni}_{0.5}\text{Zn}_{0.5}\text{Fe}_2\text{O}_4$  magnetic core was coated with PANI and a core/shell nanostructure was formed. To verify the formation of Ni-Zn ferrite in the prepared magnetic nanoparticles, the XRD pattern of the sample was investigated. The XRD patterns (Figure 4) showed that  $\text{Ni}_{0.5}\text{Zn}_{0.5}\text{Fe}_2\text{O}_4$  nanoparticles have a spinel framework with all the main peaks compatible with the  $\text{Ni}_{0.5}\text{Zn}_{0.5}\text{Fe}_2\text{O}_4$  standard pattern (JCPDS 08-0234). The adsorbent particle size was investigated using SEM. The SEM photograph of the sample (Figure 5) showed that the average size of  $\text{Ni}_{0.5}\text{Zn}_{0.5}\text{Fe}_2\text{O}_4/\text{PANI}$  is slightly less than 100 nm. The magnetic properties of the  $\text{Ni}_{0.5}\text{Zn}_{0.5}\text{Fe}_2\text{O}_4/\text{PANI}$  were evaluated using a VSM. As shown in Figure 6, the saturation magnetic moments of the  $\text{Ni}_{0.5}\text{Zn}_{0.5}\text{Fe}_2\text{O}_4/\text{PANI}$  reached about 17 emu/g. It showed superparamagnetic behavior that would enable easy recovery of the adsorbent from solution under an applied magnetic field.

The time efficacy on the phosphate removal was studied with an initial phosphate concentration of 5 mg/L. As can be seen in Figure 7, the percentage of adsorptions increased with increases in contact time. The least removal

occurred in 5 minutes (63.0%), and maximum adsorption was 69.0% at the time of 30 minutes. The process showed a fast phosphate adsorption. The adsorption level, however, reached a stable stage as time was increased, because all accessible positions were occupied.

The phosphate adsorption clearly increased with decreases in pH. When the pH was low, the positive charge on the surface of PANI was concentrated, leading to a static electricity force between positive PANI surfaces and negative phosphate ions. Then the mechanism of phosphate ion removal may be related to the electrostatic force as well as the interaction of ion-exchange (31). At a low pH, the phosphate anions can be present in solution as  $\text{HPO}_4^{-2}$  or  $\text{H}_2\text{PO}_4^-$  as follows:



PANI in the doped state (having releasable dopants such as  $\text{Cl}^-$ ) can be conveniently exchanged with anions like phosphate which exist in anionic form in aqueous solutions. At pH values higher than 3, a de-doping process took place in the polymer (PANI), and at  $\text{pH} > 5$  the desorption of phosphate becomes the significant process, lowering the amount of phosphate removed (32).

Figure 9 indicates that, when the amount of  $\text{Ni}_{0.5}\text{Zn}_{0.5}\text{Fe}_2\text{O}_4/\text{PANI}$  was increased, the percentage of adsorption also increased and approached saturation stage, where increases in  $\text{Ni}_{0.5}\text{Zn}_{0.5}\text{Fe}_2\text{O}_4/\text{PANI}$  extent did not alter phosphate removal. An increment in removal level with  $\text{Ni}_{0.5}\text{Zn}_{0.5}\text{Fe}_2\text{O}_4/\text{PANI}$  quantity could be ascribed to the enhanced space and accessibility of further adsorption sites.

Batch adsorption experiments were performed at different initial phosphate concentrations. As shown in Figure 10, these observations can be explained by the fact that increasing the initial phosphate concentration made more phosphate ions available, while the amount of active sites on the adsorbent remained constant which led to a lower removal efficiency percent.

The adsorption isotherm is important for determining the adsorption behavior of an adsorbent. The experimental data corresponded with the Langmuir, Freundlich, and Dubinin–Radushkevich models as shown in Table 1.

In the Dubinin–Radushkevich model, for  $E < 8 \text{ kJ mol}^{-1}$ , the adsorption process might be performed physically, while chemical adsorption occurs when  $E > 8 \text{ kJ mol}^{-1}$  (33). All parameters are listed in Table 1. Looking at Table 1 in which the Langmuir, Freundlich, and D–R isotherm constants for the adsorption of phosphate are summarized, it can be derived from  $R^2$  that the Freundlich model matched the experimental data better than either the Langmuir or D–R models. Moreover, it is clear that the adsorption of phosphate by  $\text{Ni}_{0.5}\text{Zn}_{0.5}\text{Fe}_2\text{O}_4/\text{PANI}$  may be explained as a physical adsorption process, for the value of  $E$  is 2.236 kJ.

Adsorption capacity is a significant parameter which determines the performance of an adsorbent. Table 2 compares the maximum adsorption capacity of  $\text{Ni}_{0.5}\text{Zn}_{0.5}\text{Fe}_2\text{O}_4/\text{PANI}$  for phosphate adsorption with that

**Table 1.** Langmuir, Freundlich, D–R isotherm constants for the adsorption of phosphate ions onto  $\text{Ni}_{0.5}\text{Zn}_{0.5}\text{Fe}_2\text{O}_4/\text{PANI}$

Langmuir			
$q_m$ ( $\text{mg g}^{-1}$ )	$K_L$	$R_L$	$R^2$
85.40	0.0096	0.51	0.931
Freundlich			
1/n	$K_F$		$R^2$
0.47	1.07		0.997
Dubinin–Radushkevich (D–R)			
$q_m$ ( $\text{mg g}^{-1}$ )	$\beta$ ( $\text{mol}^2 \text{kJ}^{-2}$ )	$R^2$	$E$ ( $\text{kJ mol}^{-1}$ )
3.57	$1 \times 10^{-7}$	0.687	2.236

**Table 2.** Maximum adsorption capacity of different adsorbents for phosphate removal

Adsorbents	$q_m$ ( $\text{mg/g}$ )	References
Modified fly ash	12.69	(34)
Magnetic biochar	1.24	(35)
Magnetic iron oxide	5.03	(36)
$\text{ZnCl}_2$ -activated carbon	5.1	(37)
Hydroxy-aluminum pillared bentonite	12.7	(38)
Metal-loaded orange waste	14	(39)
Ground burnt patties	0.41	(40)
Zeolite	2.15	(41)
$\text{Ni}_{0.5}\text{Zn}_{0.5}\text{Fe}_2\text{O}_4/\text{PANI}$	85.40	Present study

of other adsorbents in the literature.

## Conclusion

$\text{Ni}_{0.5}\text{Zn}_{0.5}\text{Fe}_2\text{O}_4/\text{PANI}$  magnetic nanoparticles were used in the adsorption of phosphate ions from aqueous solutions. The study demonstrated that the adsorption of phosphate increased with decreases in pH and was enhanced with increments in the extent of  $\text{Ni}_{0.5}\text{Zn}_{0.5}\text{Fe}_2\text{O}_4/\text{PANI}$ . Maximum phosphate adsorption was achieved at pH 5 with a maximum adsorption capacity of 85.40 mg/g at 298 K. The adsorption isotherm fit the Freundlich model well. The manufactured  $\text{Ni}_{0.5}\text{Zn}_{0.5}\text{Fe}_2\text{O}_4/\text{PANI}$  nanoparticles could be spread in the solution well and simply collected by a magnet. The water treatment described here is efficient using  $\text{Ni}_{0.5}\text{Zn}_{0.5}\text{Fe}_2\text{O}_4/\text{PANI}$ . The current results provide a practical way for water treatment and the removal of phosphate ions.

## Acknowledgments

Financial support from the Islamic Azad University-Bandar Abbas Branch (No. 11450515932016) is gratefully acknowledged.

## Ethical issues

The authors hereby certify that all data collected during the study is as stated in this manuscript, and no data from the study has been or will be published elsewhere separately.

### Competing interests

The authors declare that they have no competing interests.

### Authors' contributions

All authors contributed equally and were involved in the study design, data collection, and article approval.

### References

- Can MY, Yildiz E. Phosphate removal from water by fly ash: Factorial experimental design. *J Hazard Mater* 2008; 135(1-3): 165-70. doi: 10.1016/j.jhazmat.2005.11.036.
- Tillotson S. Phosphate removal: an alternative to chemical dosing. *Filtr Separat* 2006; 43(5): 10-2. doi: 10.1016/S0015-1882(06)70884-9.
- İrdemez Ş, Yildiz YŞ, Tosunoğlu V. Optimization of phosphate removal from wastewater by electrocoagulation with aluminum plate electrodes. *Sep Purif Technol* 2006; 52(2): 394-401. doi: 10.1016/j.seppur.2006.05.020.
- Karageorgiou K, Paschalis M, Anastassakis GN. Removal of phosphate species from solution by adsorption onto calcite used as natural adsorbent. *J Hazard Mater* 2007; 139(3): 447-52. doi: 10.1016/j.jhazmat.2006.02.038.
- Pengthamkeerati P, Satapanajaru T, Chularuengsoarn P. Chemical modification of coal fly ash for the removal of phosphate from aqueous solution. *Fuel* 2008; 87(12): 2469-76. doi: 10.1016/j.fuel.2008.03.013.
- Huang W, Wang S, Zhu Z, Li L, Yao X, Rudolph V, et al. Phosphate removal from wastewater using red mud. *J Hazard Mater* 2008; 158(1): 35-42. doi: 10.1016/j.jhazmat.2008.01.061.
- Guan XH, Chen GH, Shang C. Adsorption behavior of condensed phosphate on aluminum hydroxide. *J Environ Sci* 2007; 19(3): 312-18. doi: 10.1016/S1001-0742(07)60051-5.
- Persson P, Nilsson N, Sjöberg S. Structure and bonding of orthophosphate ions at the iron oxide-aqueous interface. *J Colloid Interface Sci* 1996; 177(1): 263-75. doi: 10.1006/jcis.1996.0030.
- Chitrakar R, Tezuka S, Sonod A, Sakane K, Ooi K, Hirotsu T. Selective adsorption of phosphate from seawater and wastewater by amorphous zirconium hydroxide. *J Colloid Interface Sci* 2006; 297(2): 426-33. doi: 10.1016/j.jcis.2005.11.011.
- Mustafa S, Zaman MI, Khan S. pH effect on phosphate sorption by crystalline MnO<sub>2</sub>. *J Colloid Interface Sci* 2006; 301(2): 370-75. doi: 10.1016/j.jcis.2006.05.020.
- Malakootian M, Yousefi N, Jaafarzadeh Haghighifard N. Kinetics modeling and isotherms for adsorption of phosphate from aqueous solution by modified clinoptilolite. *Water and Wastewater* 2011; 22(4): 21-9. [In Persian].
- Khezri SM, Majidi G, Jafari Mansoorian H, Ansari M, Atabi F, Tohidi Mogaddam T, et al. Efficiency of horizontal roughing filter in removing nitrate, phosphate and chemical oxygen demand from effluent of waste stabilization pond. *Environ Health Eng Manag J* 2015; 2(2): 87-92.
- Shen Y, Tang J, Nie Z, Ren Y, Wang Y, Zuo L. Preparation and application of magnetic Fe<sub>3</sub>O<sub>4</sub> nanoparticles for wastewater purification. *Sep Purif Technol* 2009; 68(3): 312-19. doi: 10.1016/j.seppur.2009.05.020.
- Cho DW, Jeon BH, Chon CM, Kim Y, W. Schwartz F, Lee ES, et al. A novel chitosan/clay/magnetite composite for adsorption of Cu (II) and As (V). *Chem Eng J* 2012; 200-202: 654-62. doi: 10.1016/j.cej.2012.06.126.
- Shi G. Synthesis of SiO<sub>2</sub>/Fe<sub>3</sub>O<sub>4</sub> nanomaterial and its application as cataluminescence gas sensor material for ether. *Sensors and Actuators B: Chemical* 2012; 171-172: 699-04. doi: 10.1016/j.snb.2012.05.059.
- Dallas P, Georgakilas V, Niarchos D, Komninou P, Kehagias T, Petridis D. Synthesis, characterization and thermal properties of polymer/magnetite nanocomposites. *Nanotechnology* 2006; 17(8): 2046.
- Mohan D, Sarswat A, Singh VK, Alexandre-Franco M, Pittman C. Development of magnetic activated carbon from almond shells for trinitrophenol removal from water. *Chem Eng J* 2011; 172(2-3): 1111-25. doi: 10.1016/j.cej.2011.06.054.
- Nitayaphat W, Jintakosol T. Removal of silver (I) from aqueous solutions by chitosan/bamboo charcoal composite beads. *J Clean Prod* 2015; 87(1): 850-55. doi: 10.1016/j.jclepro.2014.10.003.
- Sharma S, Verma K, Chaubey U, Singh V, Mehta BR. Influence of Zn substitution on structural, microstructural and dielectric properties of nanocrystalline nickel ferrites. *Mat Sci Eng B* 2010; 167(3): 187-92. doi: 10.1016/j.mseb.2010.02.015.
- Virden A, O'Grady K. Structure and magnetic properties of NiZn ferrite nanoparticles. *J Magn Magn Mater* 2005; 290-291(Pt 2): 868-70. doi: 10.1016/j.jmmm.2004.11.398.
- Zeng XR, Ko TM. Structures and properties of chemically reduced polyanilines. *Polymer* 1998; 39(5): 1187-95. doi: 10.1016/S0032-3861(97)00381-9.
- Kang ET, Neoh KG, Tan KL. Polyaniline: a polymer with many interesting intrinsic redox states. *Prog Polym Sci* 1998; 23(2): 277-324.
- Negi YS, Adhyapak P. Development in polyaniline conducting polymers. *J Macromol Sci Polymer* 2002; 42(1): 35-53. doi: 10.1081/MC-120003094.
- Cao Y, Andreatta A, Heeger AJ, Smith P. Influence of chemical polymerization conditions on the properties of polyaniline. *Polymer* 1989; 30(12): 2305-11. doi: 10.1016/0032-3861(89)90266-8.
- Chiang JC, MacDiarmid AG. 'Polyaniline': protonic acid doping of the emeraldine form to the metallic regime. *Synthetic Met* 1986; 13(1-3): 193-205. doi: 10.1016/0379-6779(86)90070-6.
- Gabal MA, El-Shishtawy RM, Al Angari YM. Structural and magnetic properties of nano-crystalline Ni-Zn ferrites synthesized using egg-white precursor. *J Magn Magn Mater* 2012; 324(14): 2258-64. doi: 10.1016/j.jmmm.2012.02.112.
- Stejskal J, Trchová M, Brodinová J, Fedorova SV, Prokes J, Zemek J. Coating of zinc ferrite particles with a conducting polymer, polyaniline. *J Colloid Interface Sci* 2006; 298(1): 87-93. doi: 10.1016/j.jcis.2005.12.034.
- Pol VG, Daemen LL, Vogel S, Chertkov G. Solvent-free fabrication of ferromagnetic Fe<sub>3</sub>O<sub>4</sub> octahedral. *Ind Eng Chem Res* 2009; 49(2): 920-24. doi: 10.1021/ie9011062.
- Khan JA, Qasim M, Singh BR, Singh S, Shoeb M, Khan W, et al. Synthesis and characterization of structural, optical, thermal and dielectric properties of polyaniline/CoFe<sub>2</sub>O<sub>4</sub> nanocomposites with special reference to photocatalytic activity. *Spectrochim Acta A Mol Biomol Spectrosc* 2013; 109: 313-21. doi: 10.1016/j.saa.2013.03.011.
- Stejskal J, Gilbert RG. Polyaniline, preparation of a conducting polymer (IUPAC technical report). *Pure Appl Chem* 2002; 74(5): 857-67. doi: 10.1351/pac200274050857.

31. Long F, Gong JL, Zeng GM, Chen L, Wang XY, Deng JH, et al. Removal of phosphate from aqueous solution by magnetic Fe-Zr binary oxide. *Chem Eng J* 2011; 171(2): 448-55. doi: 10.1016/j.cej.2011.03.102.
32. Ansari R. Application of polyaniline and its composites for adsorption/recovery of chromium (VI) from aqueous solutions. *Acta Chim Slov* 2006; 53: 88-94.
33. Tan Y, Chen M, Hao Y. High efficient removal of Pb (II) by amino-functionalized  $Fe_3O_4$  magnetic nanoparticles. *Chem Eng J* 2012; 191: 104-11. doi: 10.1016/j.cej.2012.02.075.
34. Xu K, Tao H, Deng T. Removal of phosphate from coating wastewater using magnetic Fe-Cu bimetal oxide modified fly ash. *Journal of Water Reuse and Desalination* 2016; 6(3) 430-6. doi: 10.2166/wrd.2015.105.
35. Chen B, Chen Z, Lv S. A novel magnetic biochar efficiently sorbs organic pollutants and phosphate. *Bioresour Technol* 2011; 102(2): 716-23. doi: 10.1016/j.biortech.2010.08.067.
36. Yoon SY, Lee CG, Park JA, Kim JH, Kim SB, Lee SH, et al. Kinetic, equilibrium and thermodynamic studies for phosphate adsorption to magnetic iron oxide nanoparticles. *Chem Eng J* 2014; 236: 341-47. doi: 10.1016/j.cej.2013.09.053.
37. Namasivayam C, Sangeetha D. Equilibrium and kinetic studies of adsorption of phosphate onto  $ZnCl_2$  activated coir pith carbon. *J Colloid Interface Sci* 2004; 280(2): 359-65. doi: 10.1016/j.jcis.2004.08.015.
38. Yan LG, Xu YY, Yu HQ, Xin XD, Wei Q, Du B. Adsorption of phosphate from aqueous solution by hydroxy-aluminum, hydroxy-iron and hydroxy-iron-aluminum pillared bentonites. *J Hazard Mater* 2010; 179(1-3): 244-50. doi: 10.1016/j.jhazmat.2010.02.086.
39. Biswas BK, Inoue K, Ghimire KN, Harada H, Ohto K, Kawakita H. Removal and recovery of phosphorus from water by means of adsorption onto orange waste gel loaded with zirconium. *Bioresour Technol* 2008; 99(18): 8685-90. doi: 10.1016/j.biortech.2008.04.015.
40. Rout PR, Bhunia P, Dash RR. Modeling isotherms, kinetics and understanding the mechanism of phosphate adsorption onto a solid waste: ground burnt patties. *J Environ Chem Eng* 2014; 2(3): 1331-42. doi: 10.1016/j.jece.2014.04.017.
41. Sakadevan K, Bavor HJ. Phosphate adsorption characteristics of soils, slags and zeolite to be used as substrates in constructed wetland systems. *Water Res* 1998; 32(2): 393-99. doi: 10.1016/S0043-1354(97)00271-6.